JOURNAL OF AIRCRAFT
Vol. 43, No. 4, July–August 2006

Analysis Tools for the Detection of Intermittent Nonlinear Aeroelastic Phenomena

Christopher C. Chabalko,* Zhongfu Ge,* and Muhammad R. Hajj†
Virginia Polytechnic Institute and State University, Blacksburg, Virginia 24061
and
Walter A. Silva‡
NASA Langley Research Center, Hampton, Virginia 23681

The nonlinear coupling between the aerodynamic load and structural motions in the experiments conducted in the Langley Transonic Dynamics Tunnel at NASA Langley Research Center on a flexible semispan model (FSM) of a high-speed civil transport wing configuration is examined. The results show that, right before "hard" flutter took place, the aerodynamic load and the structural motion of the FSM were intermittently and quadratically coupled. Particularly, the shock motion, which can be caused by local and intermittent flow separation, is nonlinearly related to the structural motion in such a manner that one full cycle of the shock motion is related to two cycles of the acceleration of the wing tip. Because of the required averaging in implementing them, Fourier-based higher-order spectral moments could not characterize this coupling. On the other hand, the wavelet-based cross bicoherence is established as a tool that is capable of detecting intermittent or transient nonlinear aeroelastic phenomena as would be encountered in model studies or flight tests.

I. Introduction

NONLINEAR aeroelastic phenomena include nonlinear physical mechanisms that arise from 1) the aerodynamic load in different flow regimes, 2) flexible components that may undergo large deformations, and/or 3) the interaction of the structure with the surrounding flowfield.[1] The complexities involved in these phenomena present the need to develop analysis tools capable of characterizing these mechanisms through the detection of nonlinearities in surface pressures, structural strains, and accelerations signals as would be measured in model studies and flight tests. Because calibrated and/or accepted errors from linear aeroelastic analysis will not be acceptable for many future vehicles,[2] there is a continuous effort to develop and refine computational aeroelastic methods to include transonic and separated flow effects and structural nonlinearities. Because these aspects are nonlinear, the validation of any computational methodology that aims at their characterization must be performed with tools capable of detecting and identifying nonlinear phenomena. Consequently, the development of nonlinear analysis tools provides a benchmark for a physics-based validation of computational methodologies against experimental measurements. Moreover, such tools can assist in the development of reduced-order models for the different nonlinear aeroelastic phenomena. Additionally, any physical insights gained through the application of these tools could yield new capabilities to improve aircraft performance and reduced uncertainties for the operation beyond conventional boundaries that are based on linear analysis. Such improvements could be attained through modifications in the design phases and/or through additions of different control systems.

Experiments conducted by Silva et al.[3] on a flexible semispan model (FSM) of a high-speed civil transport (HSCT) wing configuration and the extensive measurements of wing tip accelerations, bending, and torsional stresses and surface pressures at different locations provide a database that can be used to confirm the capabilities of different analysis tools to identify and characterize nonlinear aeroelastic phenomena. In those experiments, "hard" flutter, whereby boundless wing-tip oscillations took place, was encountered, which resulted in the loss of the model. Hajj and Silva[4] used Fourier-based auto- and cross-bispectral moments to identify nonlinear couplings in the aerodynamic load associated with a strong shock that developed near the trailing edge. This coupling could be detected only in the last available record before hard flutter took place. Consequently, one could associate such a nonlinear phenomenon with the hard flutter and argue for the possible use of such quantities to detect flutter. Bispectral analysis has also been used to identify and characterize limit-cycle oscillations on other lifting surfaces.[5–7] Chabalko et al.[8] conducted time/frequency analysis of the fluctuations measured by the pressure taps over the 95% span station and the strain gauges placed at the midspan. The results showed that, in the flow conditions leading to the hard flutter, the pressure fluctuations at the leading and trailing edges near the wing tip contained different frequency components that also showed a high level of variations with time. Additionally, the 2–1 ratio between these frequency components suggested the possibility of a quadratic interaction between the aerodynamic load and the structural response, which suggested the possibility of nonlinear structural coupling.

The objectives of this work are twofold. The first is to identify the nonlinear coupling between the aerodynamic load, as measured by one of the pressure taps close to the trailing edge near the wing tip, and the structural motion as measured by an accelerometer also placed at the trailing edge near the wing tip in the experiments of Silva et al.[3] as the hard flutter conditions were approached. The second is to establish the wavelet-based cross bicoherence as a tool capable of detecting intermittent nonlinear coupling between the aerodynamic load and the structural response and to show how physical insights can be gained from the application of this tool to characterize aeroelastic phenomena. This latter objective is based on our previous results,[8] which showed time-varying characteristics of both pressure and acceleration signals as the hard flutter conditions were approached.

II. Experimental Setup

The experiments were conducted in the Langley Transonic Dynamics Tunnel (TDT) at NASA Langley Research Center. The TDT is specially configured for flutter testing, with excellent model

Presented as Paper 2005-1858 at the AIAA/ASME/AHS/ASCE 46th Structures/Structural Dynamics and Materials Conference, Austin, TX, 18–21 April 2005; received 11 May 2005; accepted for publication 11 October 2005.

*Graduate Research Assistant, Engineering Science and Mechanics.
†Professor, Engineering Science and Mechanics.
‡Senior Research Scientist, Aeroelasticity Branch. Associate Fellow AIAA.

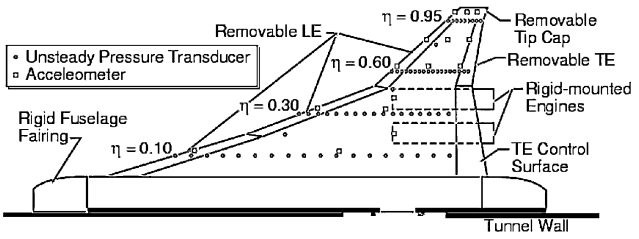

Fig. 1 Planform and instrumentation layout for FSM wind-tunnel model.

visibility from the control room and a rapid tunnel shutdown capability for model safety (bypass valves). The model planform[3] was a 1/12th-scale configuration based on an early design known as the reference H configuration. To accommodate pressure instrumentation at the wing tip of the model, the original reference H airfoil thickness was increased to a constant 4% thickness over the entire wing span. Figure 1 shows the planform layout and main components of the model. The leading and trailing edges were removable to access pressure instrumentation in those regions. A removable tip cap allowed access to pressure instrumentation at the wing tip. Note that the FSM was not intended to be a flutter clearance model but, rather, a model that would exhibit an HSCT-like flutter mechanism within the range of operation of the TDT. To induce flutter at around 200 psf, a 2.2-lb. mass was added to the aft tip section. This mass was fabricated out of tungsten and bonded into the outboard removable trailing-edge section of the FSM (Fig. 1). Additional reinforcements and local strengthening of the attachment surface between the main wing box and the outboard removable trailing-edge section was performed to handle the added stress of the additional mass.

The instrumentation layout consisted of 131 in situ unsteady pressure transducers located at the 10, 30, 60, and 95% span stations (Fig. 1). Six additional unsteady pressure transducers were installed at the 20% chord station for the 20, 45, and 75% span stations for both upper and lower surfaces. Channels were carved into the foam core to accommodate the wiring for the instrumentation. Specially designed pressure transducer holders were used to eliminate any leakage around the transducer and to provide easy access to the transducers. Instrumentation also included 14 accelerometers installed throughout the wing (Fig. 1), three of which were located close to the leading edge, midchord, and trailing edge near the wing tip. The FSM was also instrumented with three bending strain gauges and one torsion strain gauge.

III. Analysis Tools for Detection of Intermittent Nonlinear Coupling

Fourier-domain analysis is usually performed to determine fluctuation characteristics of stationary signals. Yet such analysis fails in cases where the interest is in specific events that take place over relatively short time periods. In comparison, the wavelet representation is more advantageous in the analysis of nonstationary signals. This is because the wavelet analysis preserves time-varying characteristics by mapping a temporal signal onto both time and scale domains. This makes it possible to characterize intermittent events that are covered by a data segment from both temporal and spectral perspectives. In this work, wavelet-based higher-order spectral moments, as will be described, are used to detect linear and nonlinear intermittent couplings between aerodynamic loads and structural response in the time records leading to the hard flutter of the FSM of HSCT.

A. Fourier-Based Higher-Order Spectral Analysis

The most common Fourier analysis domain is based on the auto- and cross spectrum and linear coherence, which, respectively, yield estimates of energy content of the different frequency components in a signal and the level of coherence between equal frequency components in two signals. In addition, one can use a hierarchy of higher-order spectral moments[9] to obtain quantities relevant to the identification of nonlinear relations between frequency components. For instance, the bispectrum,[10,11] which is the next higher-order moment to the power spectrum, is used to detect quadratic coupling between two frequency components and their algebraic sum. It does so through assessing the phase relation between these components. For three frequency components, f_i, f_j and their algebraic sum $f_i + f_j$, the autobispectrum of a zero-mean real signal $x(t)$ is estimated as

$$B_{xxx}(f_i, f_j) = \lim_{T\to\infty} (1/T) E[\hat{x}(f_i + f_j)\hat{x}^*(f_i)\hat{x}^*(f_j)] \quad (1)$$

where $\hat{x}$ is the Fourier transform of $x(t)$, T is the time duration of the signal $x(t)$, $E[\cdots]$ is a time average, and $(\cdots)^*$ represents the complex conjugate. Similarly, the cross bispectrum between two frequency components at f_i and f_j in one signal $x(t)$ and their sum component at $f_i + f_j$ in another signal $y(t)$ is estimated as

$$B_{xyy}(f_i, f_j) = \lim_{T\to\infty} (1/T) E[\hat{x}(f_i + f_j)\hat{y}^*(f_i)\hat{y}^*(f_j)] \quad (2)$$

In both Eqs. (1) and (2), f_i f_j and their sum are arbitrary frequencies limited by the Nyquist frequency f_N. If the three frequency components at f_i, f_j, and $f_i + f_j$ are independent, that is, each mode is characterized by a statistically independent random phase, the bispectrum will have a near-zero value after the statistical averaging is carried out. On the other hand, if the three modes are coupled through a quadratic interaction mechanism, a phase coherence will exist among them. Under these conditions, the averaging will lead to a large value for the bispectrum. The bispectrum, thus, preserves the phase information between coupled frequency components in the form of a phase relation, which could not be obtained from the power spectrum. Because of this capability, the bispectrum is used to identify quadratically coupled frequency components in one or more signals.[10,11]

To quantify the extent of coupling, the bispectrum is usually normalized to yield values bounded between 0 and 1. The normalized autobispectrum, referred to as autobicoherence, is defined as

$$b^2_{xxx}(f_i, f_j) = \frac{|B_{xxx}(f_i, f_j)|^2}{E\left[|\hat{x}(f_i + f_j)|^2\right] E\left[|\hat{x}(f_i)\hat{x}(f_j)|^2\right]} \quad (3)$$

Similarly, the cross bicoherence is defined as

$$b^2_{xyy}(f_i, f_j) = \frac{|B_{xyy}(f_i, f_j)|^2}{E\left[|\hat{x}(f_i + f_j)|^2\right] E\left[|\hat{y}(f_i)\hat{y}(f_j)|^2\right]} \quad (4)$$

In Eqs. (3) and (4), the triplet of frequency components at frequencies f_i, f_j, and $f_i + f_j$ are quadratically coupled if $b^2(f_i, f_j) = 1$, not quadratically coupled if $b^2(f_i, f_j) = 0$, and partially coupled if $0 < b^2(f_i, f_j) < 1$.

B. Wavelet-Based Higher-Order Spectral Analysis

1. Wavelet Transform

The continuous wavelet transform, $W(a, \tau)$, of a function $x(t)$ is defined as the inner product between $x(t)$ and the wavelet family $\Psi(a, t)$,

$$W(a, \tau) = \int_{-\infty}^{\infty} x(t)\Psi^*(a, t - \tau)\, \mathrm{d}t \quad (5)$$

As such, the wavelet coefficients $W(a, \tau)$ represent the contribution to $x(t)$ of scale a at a time τ. The wavelet family $\Psi(a, t)$ is generated from a mother wavelet $\Psi(t)$ by continuous translations of τ and dilations of a. Any real- or complex-valued function can be considered a mother wavelet as long as it satisfies the admissibility condition

$$\int_{-\infty}^{\infty} \frac{|\hat{\Psi}(\omega)|^2}{\omega} < \infty \quad (6)$$

where $\hat{\Psi}(\omega)$ is the Fourier transform of $\Psi(t)$. The admissibility condition means that the wavelet has a zero offset and finite bandwidth and gain. In the time domain, this condition is expressed as

the requirement that the wavelet has a zero mean and finite temporal support.

One common complex wavelet is the Morlet wavelet, where the mother wavelet is given by a sinusoid multiplied by a Gaussian function

$$\psi(t) = \pi^{-\frac{1}{4}} \exp(i\omega_0 t) \exp[-(t^2/2)] \tag{7}$$

In this definition, ω_0 is set equal to 6.0 to satisfy approximately the wavelet admissibility condition.

Because the Morlet wavelet function has a Gaussian distribution in the frequency domain, there is not a one-to-one correspondence between frequency and scale. However, because of the bandpass filter nature of Fourier-transformed wavelets, one can determine a relationship between the scale a and the peak frequency f of the bandpass filter corresponding to each scaled wavelet. This relation is given by

$$f = c/a \tag{8}$$

where

$$c = \left(\omega_0 + \sqrt{2+\omega_0^2}\right)\Big/ 4\pi$$

Hence, when $\omega_0 = 6.0$, $f = 0.9434/a$.

2. Wavelet-Based Spectral Moments

Similarly to the Fourier-based spectral moments as defined earlier, one can define a hierarchy of wavelet-based higher-order spectral moments.[12,13] The wavelet power spectrum is defined as

$$P_{xx}^{w}(a) = \int_T W_x^*(a,\tau) W_x(a,\tau)\, \mathrm{d}\tau \tag{9}$$

which yields the energy distribution among all scales over the integration time T. The wavelet cross spectrum, defined as

$$P_{xy}^{w}(a) = \int_T W_x^*(a,\tau) W_y(a,\tau)\, \mathrm{d}\tau \tag{10}$$

can be used to determine the level of coupling between equal scales (or frequencies) in two time series over the integration time length T. The normalized wavelet cross spectrum, namely, the wavelet linear coherence, is defined as

$$C_{xy}^{w}(a) = \frac{\left|P_{xy}^{w}(a)\right|^2}{P_{xx}^{w}(a) P_{yy}^{w}(a)} \tag{11}$$

yields a measure of the linear coherence of the same scale in two time series over the integration time length T. Similarly to the Fourier-based linear coherence, $C_{xy}^{w}(a)$ is bounded by zero and one.

Based on the definition of the autobispectrum in Eq. (1), one can define the wavelet autobispectrum as[12,13]

$$B_{xxx}^{w}(a_1,a_2) = \int_T W_x^*(a,\tau) W_x(a_1,\tau) W_x(a_2,\tau)\, \mathrm{d}\tau \tag{12}$$

where $1/a = 1/a_1 + 1/a_2$ is used to satisfy the frequency sum-rule $f = f_1 + f_2$. Additionally, the wavelet cross bispectrum between two real-time series $x(t)$ and $y(t)$ can be defined as

$$B_{yxx}^{w}(a_1,a_2) = \int_T W_y^*(a,\tau) W_x(a_1,\tau) W_x(a_2,\tau)\, \mathrm{d}\tau \tag{13}$$

The wavelet auto- and cross bispectrum can also be normalized to have values bounded between zero and one. They, respectively, yield the wavelet autobicoherence, defined as

$$\tilde{b}_{xxx}^2(a_1,a_2) = \frac{\left|B_{xxx}^{w}(a_1,a_2)\right|^2}{\left[\int_T |W_x(a_1,\tau) W_x(a_2,\tau)|^2\, \mathrm{d}\tau\right]\left[\int_T |W_x(a,\tau)|^2\, \mathrm{d}\tau\right]} \tag{14}$$

and the wavelet cross bicoherence, defined as

$$\tilde{b}_{yxx}^2(a_1,a_2) = \frac{|B_{yxx}^{w}(a_1,a_2)|^2}{\left[\int_T |W_x(a_1,\tau) W_x(a_2,\tau)|^2\, \mathrm{d}\tau\right]\left[\int_T |W_y(a,\tau)|^2\, \mathrm{d}\tau\right]} \tag{15}$$

Detailed definitions and interpretations of wavelet-based higher-order spectral moments along with comparisons of Fourier-based and wavelet-based bicoherence are given by van Millegen et al.[12]

3. Statistical Noise Level

Van Milligen et al.[12,13] pointed out that, because the wavelets of the Morlet wavelet family are not orthogonal, the wavelet coefficients are not statistically independent. This introduces statistical noise, which affects all resulting spectral moments. The statistical noise level in the wavelet-based linear coherence is estimated as

$$\epsilon\left[C_{xy}^{w}(a)\right] \approx 2[(F_s/f)(1/N)]^{\frac{1}{2}} \tag{16}$$

where N is the number of data points to be processed.

For the wavelet-based bicoherence, the noise level is estimated to be

$$\epsilon\left[\tilde{b}^2(f_1,f_2)\right] \approx \left[\frac{F_s/2}{\min(|f_1|,|f_2|,|f_1+f_2|)} \frac{1}{N}\right]^{\frac{1}{2}} \tag{17}$$

Baed on Eqs. (16) and (17), it is obvious that the statistical noise level may dominate the bicoherence spectrum at low frequencies. Hence, only the results of linear coherence or bicoherence that are larger than the local noise level can be considered with confidence.

IV. Results and Discussion

The dynamic responses that were encountered during flutter testing of the FSM are shown in Fig. 2. Silva et al.[3] provide a detailed discussion of these regions. Of particular interest is the narrow chimney region of high dynamic response that spans over a Mach number range from about 0.98 to 1.0 and a deep dynamic pressure range that starts at about 160 psf. At a Mach number of 0.979 under a dynamic pressure of about 245 psf, hard flutter took place, which resulted in the loss of the model. In this work, measurements obtained from the run at Mach number 0.95 under a dynamic pressure of 236 psf are analyzed. The analysis focuses on signals recorded at the pressure tap on the upper side at 95% of the span and 80% of the chord and by the trailing edge accelerometer near the wing tip. The pressure tap was used because it lies in the part of the wing that broke off and the accelerometer provides the nearest acceleration measurements to the pressure tap.

Figure 3 shows the Fourier-based power spectrum for the fluctuations measured at the pressure tap as estimated from eight averages each 3.75 s long and sampled at a rate of 500 Hz. The results clearly

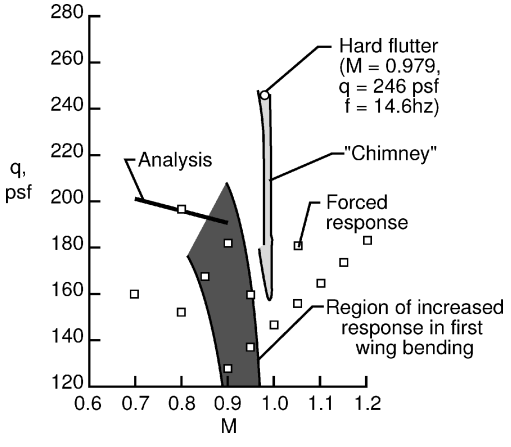

Fig. 2 Flutter and high dynamic response regions for FSM wind-tunnel model.[3]

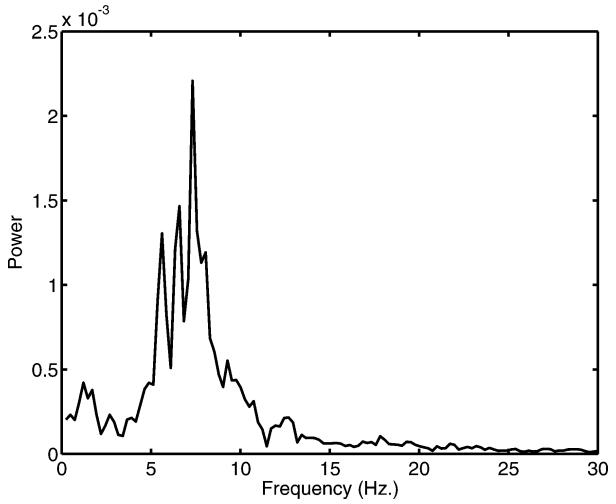

Fig. 3 Power spectrum of pressure fluctuations at tap on upper side 95% span and 80% chord.

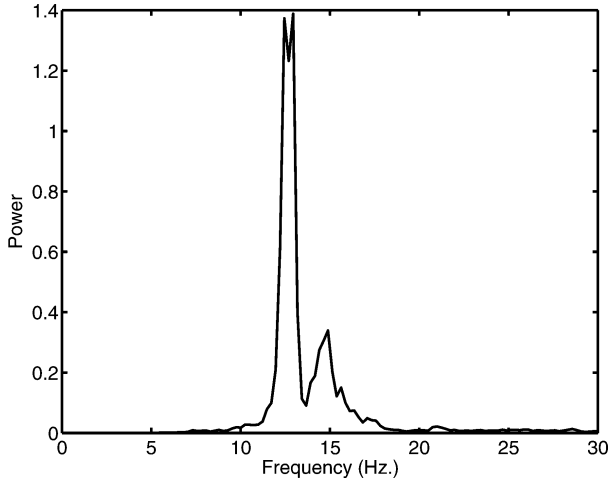

Fig. 4 Power Spectrum of acceleration signal at wing tip near trailing edge.

show three components near 5.5, 6.5, and 7 Hz, with the last component having the largest magnitude. Note that the analysis performed by Chabalko et al.[8] showed that the spectrum of the aerodynamic load on the first four taps near the leading edge, that is, up to 40% of the wing chord, exhibited high power at the high-frequency range and not at the lower ones, as exhibited at the tap located at 80% of the chord location as shown in Fig. 3. Consequently, the trailing and leading edges of the wing near the tip experienced different aerodynamic loads. The Fourier-based power spectrum of the simultaneously measured acceleration signal near the trailing edge at the wing tip is presented in Fig. 4. The spectrum exhibits a major peak around 12.5–13 Hz and a smaller one near 14 Hz. Based on these two spectra, it can be noted that the trailing edge near the wing tip experienced an aerodynamic load over a frequency range between 5.5 and 7 Hz, which resulted in a structural response over a range that is approximately twice these values. This points to the possibility of quadratic coupling between the aerodynamic load and the structural response.

The linear and quadratic coupling between the aerodynamic load and the structural response can be detected from the linear coherence and the cross bicoherence. This cross bicoherence is defined in Eq. (4). Figure 5 shows the Fourier-based linear coherence between the fluctuations measured at the pressure tap and the accelerometer signal. Note that the coherence level is about 0.4 at the dominant frequency of the structural response near 14 Hz (Fig. 4). This indicates that the relation between the aerodynamic load and the structural response is not linear. The Fourier-based cross bicoherence

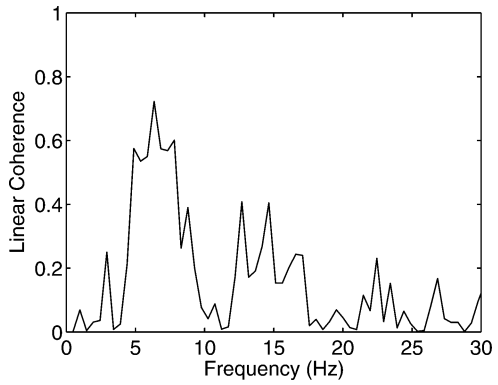

Fig. 5 Fourier-based linear coherence between pressure and acceleration signals.

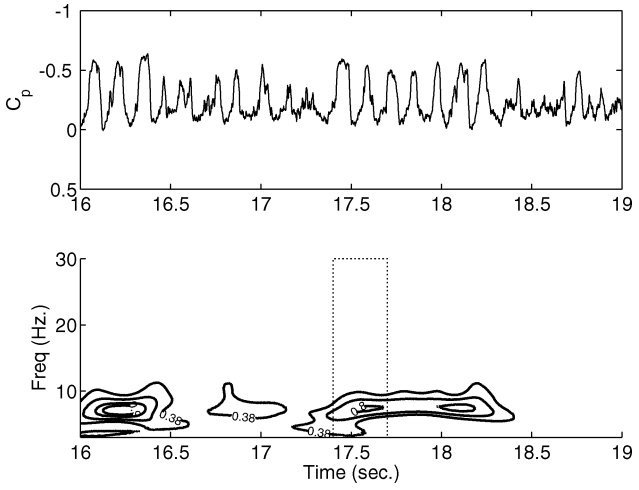

Fig. 6 Wavelet energy and time variations of pressure signal between 16 and 19 s.

between the pressure and acceleration signals was also estimated. The results showed levels that are below 0.3 for all frequency pairs in the whole bicoherence spectrum, which indicated no significant quadratic coupling over the whole record. The 2–1 ratio between the frequency components in the acceleration and pressure signals and the lack of high Fourier-based cross-bicoherence levels lead to the conclusion that the quadratic relation between the pressure and acceleration frequency component must be intermittent and that the time variations of this relation must be considered.

Figure 6 shows the time series of the pressure signal over the time period between 16 and 19 s along with the wavelet energy over the same period. The time signal shows significant variations over the time periods between 16 and 16.4 s, 16.4 and 17.4 s, and 17.4 and 18.2 s. The characteristic of these variations can be detected from the wavelet energy, which shows periodic variations with a frequency range between 5 and 7 Hz between 16 and 16.4 s and between 17.4 and 18.2 s. These variations are not observed over other periods of the signal. To assess the relation between the pressure and accelerometer signals, Fig. 7 shows the time series of the accelerometer signal along with the wavelet energy over the time period between 16 and 19 s. A comparison of the two time series in Figs. 6 and 7 shows simultaneous periodic variations over the time periods between 16 and 16.4 s and between 17.4 and 17.7 s. The wavelet energy in Fig. 7 shows that the periodic variations over these time periods are in the frequency range between 11 and 14 Hz.

Considering the two time series and their respective wavelet energy plots in Figs. 6 and 7, one can conclude that intermittent quadratic coupling between the two signals takes place. To assess the level of quadratic coupling between the aerodynamic load and the structural response, a window has been marked with dashed lines over each of the wavelet energy plots to mark the time integration

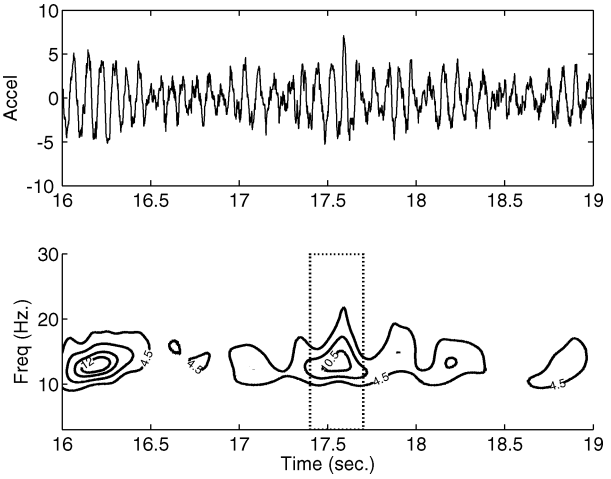

Fig. 7 Wavelet energy and time variations of accelerometer signal between 16 and 19 s.

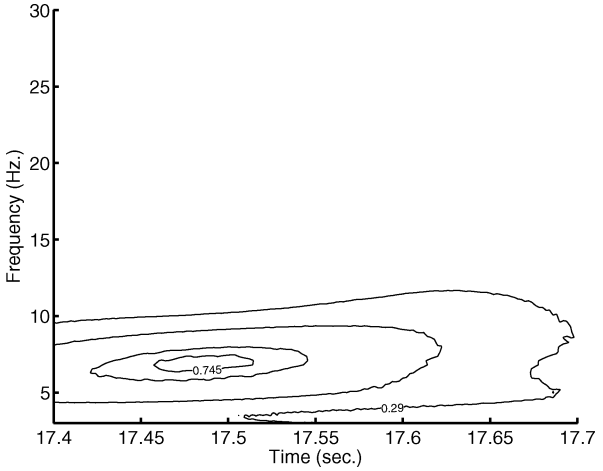

Fig. 8 Magnified portion of wavelet energy of pressure signal between 17.4 and 17.7 s.

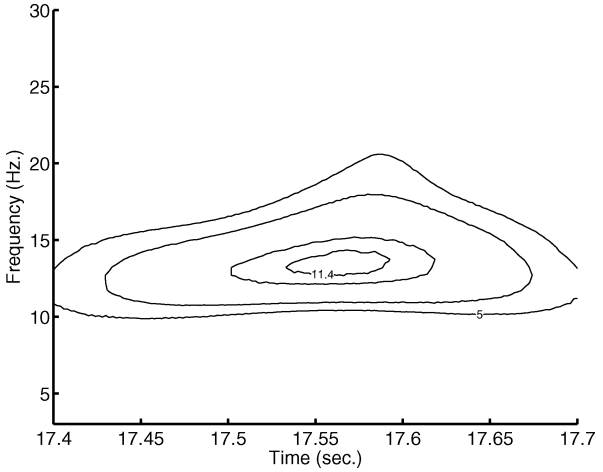

Fig. 9 Magnified portion of wavelet energy of accelerometer signal between 17.4 and 17.7 s.

limits for the wavelet linear coherence and cross bicoherence defined in Eqs. (11) and (15). The details of the windowed wavelet energy of the pressure and accelerometer signals are presented in Figs. 8 and 9.

The wavelet-based linear coherence, as defined in Eq. (11), between frequency components of the pressure and the acceleration signals is presented in Fig. 10. The solid line represents the coherence level, and the dashed line represents the noise threshold.

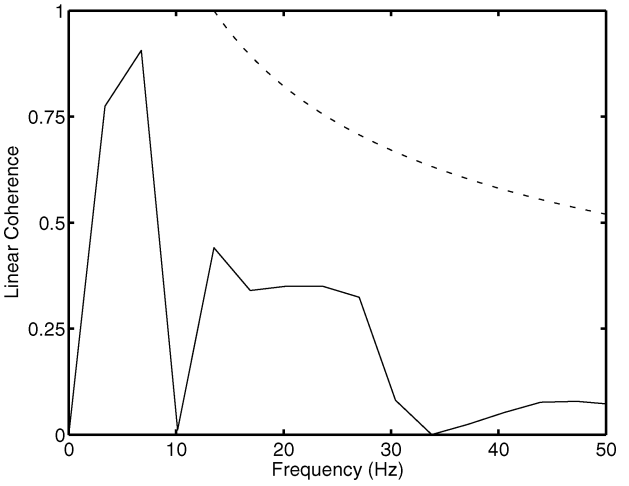

Fig. 10 Wavelet-based linear coherence between pressure and acceleration between 17.4 and 17.7 s.

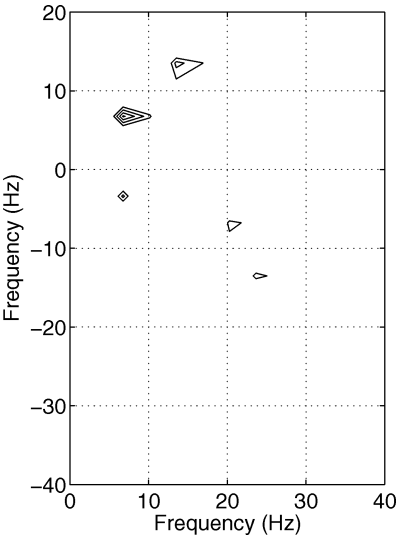

Fig. 11 Wavelet-based cross-bicoherence between pressure and acceleration between 17.4 and 17.7 s with contour levels set at 0.6, 0.7, 0.8, and 0.9.

Although there is high level of linear coherence near 7 Hz, it is obvious that the coherence level is well below the noise level. Consequently, the analysis shows no clear linear coherence.

The quadratic coupling between frequency components in the pressure signal and their algebraic sum in the acceleration signal is shown in the contour plot of the wavelet-based cross-bicoherence presented in Fig. 11. In this plot, the contour level at the frequency pair f_1 along the horizontal axis and f_2 along the vertical axis represents the value of the cross-bicoherence between f_1, f_2 and their sum $f_1 + f_2$. Only cross-bicoherence levels above the noise threshold, as defined in Eq. (17), are plotted. The results show a high level of cross bicoherence ($\simeq$0.9) over (7 Hz, 7 Hz), which indicates self-coupling of the frequency range near 7 Hz in the pressure signal and their sum near 14 Hz in the accelerometer signal. Slightly lower values of cross bicoherence (0.7) are obtained over (14 Hz, 14 Hz), which indicates self-coupling of the frequency range near 14 Hz in the pressure signal and their sum near 28 Hz in the accelerometer signal. Lower coupling levels are also detected over (21 Hz, -7 Hz) and its sum, 14 Hz, in the accelerometer signal. To show the intermittency of quadratic coupling between the aerodynamic load and structural motion, wavelet cross-bicoherence estimates were obtained over two other integration periods, namely, 16.1–16.4 s and 16.5–17.5 s. Figure 12, which is obtained over the first period, between 16.1 and 16.4 s, shows a high level of coherence over the

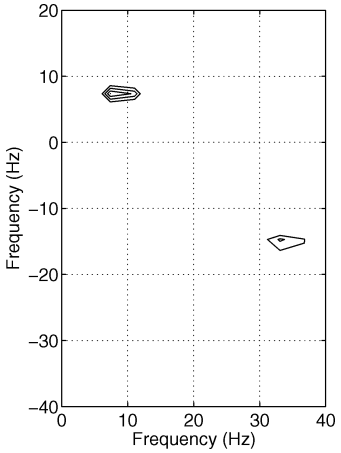

Fig. 12 Wavelet-based cross bicoherence between pressure and acceleration 16.1 and 16.4 s with contour levels set at 0.6, 0.7, 0.8, and 0.9.

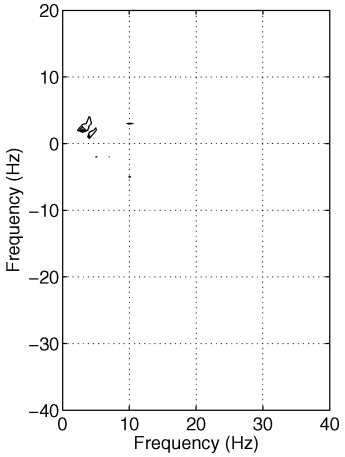

Fig. 13 Wavelet-based cross bicoherence between pressure and acceleration between 16.5 and 17.5 s with contour levels set at 0.6, 0.7, 0.8, and 0.9.

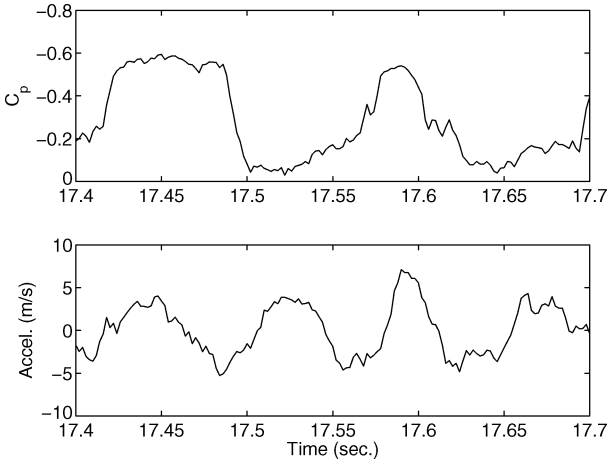

Fig. 14 Pressure and acceleration records between 17.4 and 17.7 s.

frequency range near 7 Hz in the pressure signal and the range near 14 Hz in the acceleration signal. On the other hand, Fig. 13 shows no coupling over the time period between 16.5 and 17.5 s.

The coupling can be examined further by plotting the time series of the pressure and acceleration signals during the interval of interest, that is, between 17.4 and 17.7 s. A comparison of these signals is presented in Fig. 14. The results show that, during this time period, the pressure signal goes through two periods, whereas that of the acceleration signal goes through four periods. As such, one concludes that the structural response of the trailing edge near the wing tip is related quadratically, yet intermittently, to the variation in the aerodynamic load.

Further insight into the physical aspects of the variations in the aerodynamic load can be obtained from Fig. 15, which shows the distribution of the pressure coefficient on the upper surface of the wing at different times, namely, $t_1 = 17.485$, $t_2 = 17.555$, and $t_3 = 17.62$. Corresponding acceleration magnitudes near the trailing edge of the wing tip are marked on the acceleration record presented in Fig. 15. The points denoted by a black dot in both parts of Fig. 15 correspond to $t_1 = 17.485$ s. At this time, the pressure at the 80% tap is a minimum and there is evidence that a shock formed behind the tap. The points denoted by a square show that the acceleration has gone through one cycle. On the other hand, the pressure profile on the wing shows that the shock has moved upstream to near the 40% pressure tap. The points denoted by $\times$ at $t_3 = 17.62$ s shows that the acceleration has gone through an additional cycle and the shock has moved back to near the 80% tap. Consequently, the shock motion, which can be caused by local and intermittent flow separation, is nonlinearly related to the structural motion whereby one full cycle of shock motion is related to two cycles of the acceleration of the wing tip.

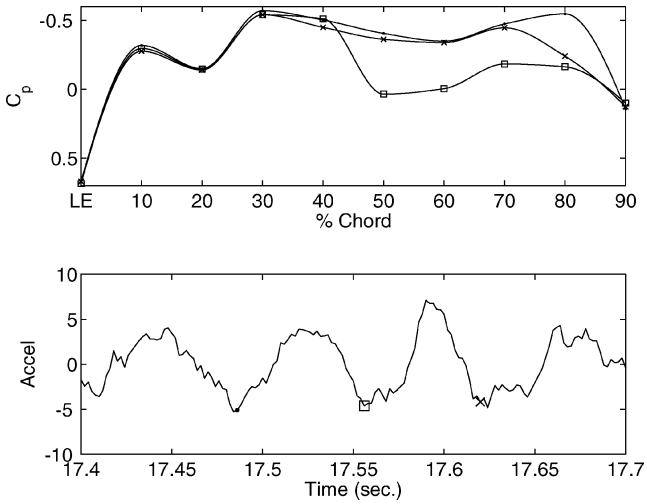

Fig. 15 Distribution of pressure coefficient near wing tip at t = 17.485, 17.555, and 17.62 s and acceleration record between 17.4 and 17.7 s.

V. Conclusions

In this work, the nonlinear couplings between the aerodynamic load and structural motions in the experiments conducted in the TDT at the NASA Langley Research Center on an FSM of an HSCT wing configuration are examined. The results show that, right before hard flutter took place, the aerodynamic load and the structural motion of the FSM were intermittently and quadratically coupled. Particularly, the results show that the shock motion, which can be caused by local and intermittent flow separation, is nonlinearly related to the structural motion in such a manner that one full cycle of the shock motion is related to two cycles of the acceleration of the wing tip. Because of the required averaging in implementing them, Fourier-based higher-order spectral moments could not characterize this coupling. On the other hand, the wavelet-based cross bicoherence is established as a tool that is capable of detecting intermittent or transient nonlinear aeroelastic phenomena as would be encountered in model studies or flight tests.

Acknowledgment

The support of the U.S. Air Force Office of Scientific Research through Grant F49620-03-1-0206 and of the National Institute of Aerospace through Grant VT-03-01, Subnumber 3044-VT Supplement 7 is acknowledged.

References

[1]Dowell, E., Edwards, J., and Strganac, T., "Nonlinear Aeroelasticity," *Journal of Aircraft*, Vol. 40, No. 5, 2003, pp. 857–874.

[2]Schuster, D. M., Liu, D. D., and Huttsell, L. J., "Computational Aeroelasticity: Sucess, Progress, Challenge," *Journal of Aircraft*, Vol. 40, No. 5, 2003, pp. 843–856.

[3]Silva, W. A., Keller, D. F., Florance, J. R., Cole, S. R., and Scott, R. C., "Experimental Steady and Unsteady Aerodynamic and Flutter Results for HSCT Semispan Models," AIAA Paper 2000-1697, April 2000.

[4]Hajj, M. R., and Silva, W. A., "Nonlinear Flutter Aspects of the Flexible HSCT Semispan Model," *Journal of Aircraft*, Vol. 41, No. 5, 2004, pp. 1202–1208.

[5]Chang, J. H., Stearman, R. O., Choi, D., and Powers, E. J., "Identification of Aeroelastic Phenomenon Employing Bispectral Analysis Techniques," *3rd International Modal Analysis Conference*, Society of Experimental Mechanics, Bethel, CT, 1985, pp. 956–964.

[6]Stearman, R. O., Powers, E. J., Schwartz, J., and Yurkovich, R., "Aeroelastic System Identification of Advanced Technology Aircraft Through Higher Order Signal Processing," *10th International Modal Analysis Conference*, Vol. 2, Society of Experimental Mechanics, Bethel, CT, 1992, pp. 1607–1610.

[7]Stearman, R. O., and Lamb, J. L., "Applications of Higher-Order Statistics to Aircraft Aeroelastic Stability and Fluid–Structural Interactions," *Higher-Order Statistical Signal Processing*, edited by B. Boashash, E. J. Powers, and A. Zoubir, Longman, Melbourne, Australia, pp. 325–379.

[8]Chabalko, C. C., Hajj, M. R., and Silva, W. A., "Time/Frequency Analysis of the Flutter of the Flexible HSCT Semispan Model," *Journal of Aircraft* (to be published).

[9]Powers, E. J., and Im, S., "Introduction to Higher-Order Statistical Signal Processing and Its Applications," *Higher-Order Statistical Signal Processing*, edited by B. Boashash, E. J. Powers, and A. Zoubir, Longman, Melbourne, Australia, pp. 381–404.

[10]Kim, Y. C., and Powers, E. J., "Digital Bispectral Analysis and its Applications to Nonlinear Wave Interactions," *IEEE Transactions in Plasma Science*, Vol. PS-7, No. 2, 1979, pp. 120–131.

[11]Hajj, M. R., Miksad, R. W., and Powers, E. J., "Perspective: Measurements and Analyses of Nonlinear Wave Interactions with Higher-Order Spectral Moments," *Journal of Fluid Engineering*, Vol. 119, No. 3, 1997, pp. 3–13.

[12]van Milligen, B. P., Sanchez, E., Estrada, T., Hidalgo, C., Brnas, B., Carreras, B., and Garcia, L., "Wavelet Bicoherence: A New Turbulence Analysis Tool," *Physics of Plasmas*, Vol. 2, No. 8, 1995, pp. 3017–3032.

[13]van Milligen, B. P., Hidalgo, C., Sanchez, E., Pedrosa, M. A., Balbin, R., Garcia-Cortes, I., and Tynan, G. R., "Statistically Robust Linear and Nonlinear Wavelet Analysis Applied to Plasma Edge Turbulence," *Review of Scientific Instruments*, Vol. 68, No. 1, 1997, pp. 967–970.